

Ergodic Spectral Efficiency in MIMO Cellular Networks

Geordie George, *Student Member, IEEE*, Ratheesh K. Mungara, *Student Member, IEEE*, Angel Lozano, *Fellow, IEEE*, and Martin Haenggi, *Fellow, IEEE*

Abstract

This paper shows how the application of stochastic geometry to the analysis of wireless networks is greatly facilitated by (i) a clear separation of time scales, (ii) abstraction of small-scale effects via ergodicity, and (iii) an interference model that reflects the receiver's lack of knowledge of how each individual interference term is faded. These procedures render the analysis both more manageable and more precise, as well as more amenable to the incorporation of subsequent features. In particular, the paper presents analytical characterizations of the ergodic spectral efficiency of cellular networks with single-user multiple-input multiple-output (MIMO) and sectorization. These characterizations, in the form of easy-to-evaluate expressions, encompass the coverage probability, the distribution of spectral efficiency over the network locations, and the average thereof.

I. INTRODUCTION

Stochastic geometry is quickly becoming an indispensable instrument in wireless network analysis. By mapping the empirical distribution of transmitter and receiver locations to appropriate point processes, it becomes possible to apply a powerful and expanding toolkit of mathematical results. This offers a complement, and increasingly even an outright alternative, to the Monte-Carlo simulations that have long been the workhorse of wireless network design.

G. George, R. K. Mungara, and A. Lozano are with the Department of Information and Communication Technologies, Universitat Pompeu Fabra (UPF), 08018 Barcelona, Spain. E-mail: {geordie.george, ratheesh.mungara, angel.lozano}@upf.edu. Martin Haenggi is with the University of Notre Dame, Notre Dame, IN 46556, USA. E-mail: mhaenggi@nd.edu. This work was supported by Project TEC2015-66228-P (MINECO/FEDER, UE), by the European Research Council under the H2020 Framework Programme/ERC grant agreement 694974, and by the U.S. NSF through award CCF 1525904.

Although a stochastic modelling of transmitter and receiver locations may seem mostly amenable to ad hoc networks, which are devoid of fixed infrastructure, a seminal paper by Andrews *et al.* [1] proved the truly remarkable effectiveness of stochastic modelling also in cellular networks—even with simple Poisson point processes (PPPs). Indeed, while it may appear that more sophisticated spatial distributions could better capture the relative regularity of actual base station (BS) placements, because of shadowing it is the case that PPPs lead to remarkably precise characterizations of signal strengths and interference, and thus of all ensuing performance measures. In fact, as shown in [2], [3] and expounded later in this paper, PPP-based characterizations represent the limit to which actual behaviors converge as the shadowing strengthens.

Altogether, the irruption of stochastic geometry is a transcendent development in wireless research, and it is reasonable to expect its importance to grow even further as networks become denser and more heterogeneous [4], [5]. Important contributions to the advancement of the discipline in the context of wireless networks include [6]–[27].

The present paper deals with the ergodic spectral efficiency of Poisson cellular networks, a quantity already tackled in works dating back to [1]. Our analysis, however, relies on a different modeling approach for the interference. This takes us on a different route, one that proves greatly advantageous because it yields solutions that are both simpler and more precise than previous ones, and, most importantly, because it opens the door to accommodating key ingredients—such as MIMO and cell sectorization—that seemed previously elusive. The modeling approach that unlocks these new analytical possibilities is not arbitrary, but rather based on sound arguments:

- 1) A clean separation between small- and large-scale channel features, in recognition that the phenomena that give rise to these features are distinct.
- 2) An unwavering embrace of ergodic performance metrics with respect to the small-scale features, in recognition that such small-scale ergodicity reflects well the operating conditions of modern wireless systems [28], [29].
- 3) The admission that each receiver can track the fading of its intended signal, but not the fading of each individual interference term.

With small- and large-scale features decoupled, ergodicity enables abstracting out the former so as to focus the stochastic geometry analysis where it makes a difference (on the large-scale aspects), reaping the most out of its potent machinery. As mentioned, this allows advancing the analysis on all fronts: tractability, accuracy, and generality. In particular, and to the extent

of our knowledge, the spectral efficiency expressions obtained in this paper are the first such characterizations that incorporate MIMO spatial multiplexing. Likewise, sectorization is also readily included.

Besides providing new expressions for quantities of interest, the present paper seeks to promote the importance of keeping the two foregoing arguments present when applying stochastic geometry to wireless networks. For conceptual clarity, these arguments are herein elaborated on the basis of a cellular network where each user is served by a single BS, and where only the downlink is considered. However, the arguments apply equally to networks featuring BS cooperation, and to the uplink, only with certain expressions suitably replaced by generalizations or counterparts.

II. NETWORK MODELLING

A. Separation of Scales

Rooted in extensive propagation measurements, the separation between large-scale propagation phenomena (distance-dependent path loss and shadowing) and small-scale multipath fading has been instrumental in the study of wireless networks since their onset, greatly facilitating characterizations that would otherwise be unwieldy [30]. The premise of this separation is that, over suitably small distances (tens to hundreds of wavelengths), the large-scale phenomena remain essentially unchanged and only small-scale variations transpire. This allows delineating local neighborhoods around transmitters and receivers wherein the small-scale channel behavior conforms to a stationary random process whose distribution is dictated by the large-scale features. Then, through the user velocity, this space-domain random process maps to a time-domain process. Moreover, under the very mild condition that the Doppler spectrum be free of delta functions, this time-domain process is ergodic.

For frequencies and velocities in the widest possible range of interest, the dwell time in a local neighborhood is far longer than the extension of signal codewords. Thus, large-scale features can be regarded as constant over an individual codeword. Alternatively, the small-scale fading may or may not remain constant over a codeword, depending on the coherence of such fading and on how codewords are arranged in time and frequency, and this dichotomy gives rise to two classic information-theoretic idealizations of the channel over the horizon of a codeword:

- *Nonergodic*. Fading random, but fixed over the codeword.

- *Ergodic*. Fading random and exhibiting sufficiently many values to essentially reveal its distribution over the codeword.

These two idealizations, in turn, map respectively to outage and ergodic definitions for the spectral efficiency. Although both are useful, the ergodic definition is the most representative in modern systems where codewords can be interspersed over very wide bandwidths, across hybrid-ARQ repetitions, and possibly over multiple antennas, and they can be subject to scheduling and link adaptation. As argued in [28], [29], the balance of these mechanisms is indeed best abstracted by ergodic spectral efficiencies involving expectations over the small-scale fading, with the large-scale features held fixed. It is at this point that stochastic geometry should enter the analysis, when the small-scale effects have been abstracted out and we can zoom out to cleanly examine the large-scale ones.

B. Large-scale Modeling

We consider the downlink of a cellular network, initially with omnidirectional antennas (to be generalized to sectorized antennas in Section VIII), where the signals are subject to path loss with exponent $\eta > 2$ and shadowing.

Suppose that the BS positions are agnostic to the radio propagation. It has been recently shown [2], [3] that, regardless of what those BS positions are (under only a very mild homogeneity condition), an increasing shadowing standard deviation σ_{dB} renders the network progressively PPP-like from the vantage of any given user, i.e., it makes the powers that a user receives from any population of BSs look as if they originated from PPP-distributed BSs. This important observation, upheld even if the shadowing is correlated [31], strongly justifies the modelling assumption of PPP-located BSs. Ironically then, shadowing, a nuisance in the study of regular geometries, simplifies the stochastic modelling of networks by making them all look alike propagation-wise regardless of their underlying geometry. And, although the convergence to a PPP behavior is asymptotic in σ_{dB} , values of interest suffice for networks to look essentially Poissonian. In particular, it is shown in [2] that, for a regular lattice of BSs spawning hexagonal cells and $\eta = 4$, $\sigma_{\text{dB}} = 12$ dB suffices to render the received powers indistinguishable (with 99% confidence in a Kolmogorov-Smirnov test) from those in a Poisson network, 90% of the time. In Section IX we provide further evidence supporting the suitability of a PPP model for the analysis of lattice networks with relevant values of σ_{dB} .

The foregoing convergence is a powerful argument in favor of a PPP model for the spatial distribution of BSs, say a process $\Phi_b \subset \mathbb{R}^2$, without the need for explicit modeling of the shadowing as it is already implicitly captured by the Poisson nature of the network. The density of Φ_b , say λ_b , depends on the type and strength of the shadowing in addition to the actual positions of the BSs [32]–[35].

Turning now to the spatial distribution of users, a good starting point is to model it as an independent PPP Φ_u with density λ_u . (This model could be refined to incorporate user clustering tendencies as well as dependences between the positions of users and BSs [36]–[39].)

Without loss of generality, the analysis can be conducted from the perspective of a user at the origin, which becomes the typical user under expectation over Φ_b . Denoting by r_k the distance between such user and the k th BS, whose location—recall—is distributed according to Φ_b , we index the BSs in increasing order of r_k , i.e., such that $r_k < r_{k+1}$ for $k \in \mathbb{N}_0$. Since, in terms of Φ_b , the only large-scale propagation mechanism at play is path loss, the user at the origin receives the strongest power from the BS at r_0 , which we deem the serving BS.

C. Small-scale Modeling

Let the communication be SISO for now, i.e., with BSs and users having a single antenna, and further let each receiver be privy to the fading of only its intended signal. Denoting by P the power measured at 1 m from a BS transmitter, at symbol n the user at the origin observes

$$y[n] = \sqrt{P r_0^{-\eta}} H_0[n] s_0[n] + z[n], \quad (1)$$

where the leading term is the intended signal from the serving BS while

$$z[n] = \sum_{k=1}^{\infty} \sqrt{P r_k^{-\eta}} H_k[n] s_k[n] + v[n] \quad (2)$$

is the aggregate interference from all other BSs, plus thermal noise v . In turn, s_k is the signal transmitted by the k th BS and H_k is the associated fading coefficient.

The fading coefficients $\{H_k\}_{k=0}^{\infty}$ are independent and of unit power, but otherwise arbitrarily distributed, while $v \sim \mathcal{N}_{\mathbb{C}}(0, N_0)$. The signal is distributed as $s_k \sim \mathcal{N}_{\mathbb{C}}(0, 1)$, a choice that is justified later.

Conditioned on $\{r_k\}_{k=0}^{\infty}$, which are fixed as far as the small-scale modeling is concerned, the instantaneous SINR at symbol n is

$$\text{SINR}[n] = \frac{P r_0^{-\eta} |H_0[n]|^2}{P \sum_{k=1}^{\infty} r_k^{-\eta} |H_k[n]|^2 + N_0}. \quad (3)$$

III. INTERFERENCE MODELING

With $H_0[1], \dots, H_0[N]$ known at the receiver, the mutual information (in bits/symbol) over codewords spanning N symbols is

$$\frac{1}{N} I(s_0[1], \dots, s_0[N]; y[1], \dots, y[N] | H_0[1], \dots, H_0[N], \{r_k\}_{k=0}^{\infty}), \quad (4)$$

which, with IID codeword symbols, becomes

$$\frac{1}{N} \sum_{n=1}^N I(s_0[n]; y[n] | H_0[n], \{r_k\}_{k=0}^{\infty}). \quad (5)$$

As argued earlier, codewords are nowadays long enough—thousands of symbols—and arranged in such a way—interspersed in time, frequency, and increasingly across antennas—so as to experience sufficiently many fading swings for an effective averaging of the mutual information to take place over the small-scale fading. From the stationarity and ergodicity of the small-scale fading over the codeword, the averaging in (5) becomes an expectation over H_0 and confers the significance of the ergodic spectral efficiency (in bits/s/Hz)

$$C_{\text{exact}} = \mathbb{E}_{H_0} \left[I(s_0; y | H_0, \{r_k\}_{k=0}^{\infty}) \right] \quad (6)$$

$$= \mathbb{E}_{H_0} \left[I \left(s_0; \sqrt{P r_0^{-\eta}} H_0 s_0 + z \mid H_0, \{r_k\}_{k=0}^{\infty} \right) \right]. \quad (7)$$

This quantity, a baseline in the sequel, does not admit explicit expressions. Rather, the evaluation of C_{exact} requires computationally very intensive Monte-Carlo simulations (cf. Appendix A) and a 64-core high-performance computing cluster is employed to generate the corresponding results throughout the paper; for all such results, 99% confidence intervals are given.

Let us examine the local distribution, for some given $\{r_k\}_{k=1}^{\infty}$, of the interference-plus-noise z as defined in (2). The first thing to note is that, without further conditioning on $\{H_k\}_{k=1}^{\infty}$, i.e., without the receiver knowing the fading coefficients from *all* interfering BSs, the distribution of z over the local neighborhood is generally not Gaussian. Conditioned only on $\{r_k\}_{k=1}^{\infty}$, the distribution of z is actually highly involved; in Rayleigh fading, for instance, it involves products of Gaussians. While the non-Gaussianity of z is irrelevant to the SINR, since only the variance

of z matters in that respect, it is relevant to information-theoretic derivations and chiefly that of the spectral efficiency, which does depend on the distribution of z .

It is nevertheless customary to analyze C_{exact} in the form it would have if $\{H_k\}_{k=1}^{\infty}$ were actually known by the receiver at the origin and z were consequently Gaussian, namely the form

$$C_{\text{ub}} = \mathbb{E}_{\{H_k\}_{k=0}^{\infty}} \left[\log_2 \left(1 + \frac{P r_0^{-\eta} |H_0|^2}{P \sum_{k=1}^{\infty} r_k^{-\eta} |H_k|^2 + N_0} \right) \right] \quad (8)$$

where the tacit—and seldom made explicit—redefinition of z as Gaussian is unmistakable from $I(s_0; \sqrt{\gamma}s_0 + z) = \log_2(1 + \gamma)$, which holds only when s_0 and z are Gaussian. As it turns out, a Gaussian modeling of z is not unreasonable because, if a decoder is intended for Gaussian interference-plus-noise (either by design or because the distribution thereof is unknown), then the spectral efficiency is precisely as if the interference-plus-noise were indeed Gaussian, regardless of its actual distribution [40]. And, once z is taken to be Gaussian, the capacity-achieving signal distribution is also Gaussian, validating our choice for s_0 . At the same time, the granting of $\{H_k\}_{k=1}^{\infty}$ as additional side information to the receiver renders (8) an upper bound to C_{exact} , hence the denomination C_{ub} .

While much more tractable than C_{exact} , the form of C_{ub} has the issue of depending not only on H_0 , but further on $\{H_k\}_{k=1}^{\infty}$. This still clutters its analysis considerably, as seen later.

Alternatively, what we propound in this paper is to model z as Gaussian, but forgoing the small-scale variations in its power, i.e., to use

$$z \sim \mathcal{N}_{\mathbb{C}} \left(0, P \sum_{k=1}^{\infty} r_k^{-\eta} + N_0 \right). \quad (9)$$

The closeness between this distribution for z and its original brethren in (2) has been tightly bounded [41], [42].

The model proposed in (9) has the virtue of rendering z Gaussian without the strain of gifting the receiver with $\{H_k\}_{k=1}^{\infty}$ and, as in other contexts where it has been tested [7], [43], [44], the result of this restraint turns out to be gratifyingly good for cellular network analysis. With z as in (9), the instantaneous SINR then becomes

$$\text{SINR} = \frac{P r_0^{-\eta} |H_0|^2}{P \sum_{k=1}^{\infty} r_k^{-\eta} + N_0}, \quad (10)$$

and the corresponding ergodic spectral efficiency is

$$C = \mathbb{E}_{H_0} \left[\log_2 \left(1 + \frac{P r_0^{-\eta} |H_0|^2}{P \sum_{k=1}^{\infty} r_k^{-\eta} + N_0} \right) \right], \quad (11)$$

which is the quantity we shall work with.

Since, with Gaussian codewords and a given $\mathbb{E}[|z|^2]$, the mutual information is minimized when z is Gaussian [45], we have that $C \leq C_{\text{exact}}$. The similarity between C and C_{exact} , with the former characterized analytically and the latter obtained through Monte-Carlo simulation, is illustrated throughout the paper.

Contrasting the instantaneous SINR expressions in (3) and (10), the analytical virtues of our model for z become evident once we rewrite the latter as $\text{SINR} = \rho |H_0|^2$, where

$$\rho = \frac{P r_0^{-\eta}}{P \sum_{k=1}^{\infty} r_k^{-\eta} + N_0} \quad (12)$$

is the local-average¹ SINR at the origin, fixed over any entire codeword and cleanly separated from the fluctuant term $|H_0|^2$; this reflects the decoupling between the large- and small-scale dependences. In interference-limited conditions ($P/N_0 \rightarrow \infty$), the local-average SINR specializes to $\rho = \frac{r_0^{-\eta}}{\sum_{k=1}^{\infty} r_k^{-\eta}}$. For given BS and user locations, ρ becomes determined and the conditional distribution of the instantaneous SINR is then given directly by that of $|H_0|^2$, i.e., by the CDF $F_{|H_0|^2}(\cdot)$, while the ergodic spectral efficiency of a user with local-average SINR ρ is

$$C(\rho) = \mathbb{E}_{H_0} \left[\log_2 (1 + \rho |H_0|^2) \right] \quad (13)$$

$$= \int_0^{\infty} \log_2(1 + \rho \xi) dF_{|H_0|^2}(\xi), \quad (14)$$

which, through ρ , sets the stage for further computations involving the geometry of the network. As anticipated, it is here where stochastic geometry can be applied with all its potency, undistracted by lingering small-scale terms.

Example 1. In Rayleigh fading, $F_{|H_0|^2}(\xi) = 1 - e^{-\xi}$, from which

$$C(\rho) = e^{1/\rho} E_1 \left(\frac{1}{\rho} \right) \log_2 e, \quad (15)$$

where $E_n(x) = \int_1^{\infty} t^{-n} e^{-xt} dt$ is an exponential integral.

For fading distributions other than Rayleigh, or with MIMO or other features, corresponding forms can be obtained for $C(\rho)$, always with the key property of these being a function of ρ and not of the instantaneous fading coefficients.

¹The term ‘‘local-average’’ indicates averaging over the small-scale fading only. It follows that the ‘‘local-average SINR’’ is its average value over a region small enough for the path loss (and the shadowing, if applicable) not to change noticeably.

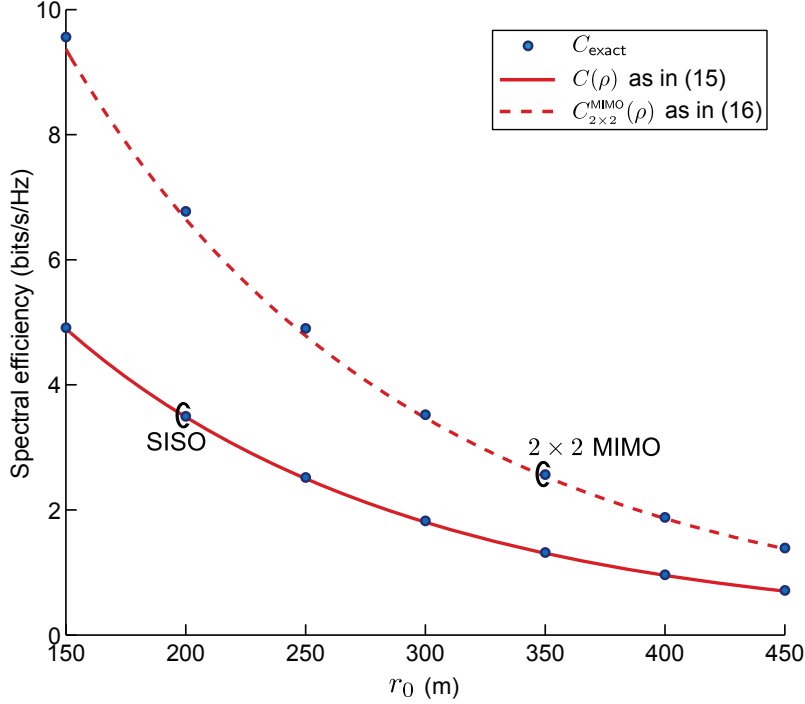


Fig. 1: Spectral efficiency vs. r_0 for $\lambda_b = 2$ BSs/km², $\eta = 3.8$ and $r_k = \frac{\Gamma(k+1.5)}{\sqrt{\pi\lambda_b} \Gamma(k+1)}$ for $k = 1, \dots, 100$. The 99% confidence intervals around C_{exact} range from ± 0.029 at $r_0 = 150$ m to ± 0.009 at $r_0 = 450$ m, for both SISO and MIMO.

Example 2. Let transmitter and receiver be equipped, respectively, with N_t and N_r antennas. If H_0 is replaced by an $N_r \times N_t$ channel matrix \mathbf{H}_0 having IID Rayleigh-faded entries, then [46]

$$C_{N_r \times N_t}^{\text{MIMO}}(\rho) = e^{N_t/\rho} \sum_{i=0}^{m-1} \sum_{j=0}^i \sum_{\ell=0}^{2j} \left\{ \binom{2i-2j}{i-j} \binom{2j+2n-2m}{2j-\ell} \cdot \frac{(-1)^\ell (2j)! (n-m+\ell)!}{2^{2i-\ell} j! \ell! (n-m+j)!} \sum_{q=0}^{n-m+\ell} E_{q+1} \left(\frac{N_t}{\rho} \right) \right\} \log_2 e \quad (16)$$

with $m = \min(N_t, N_r)$ and $n = \max(N_t, N_r)$.

Example 3. Let us consider the application of (15) to an interference-limited network with 100 interfering BSs. To typify the network, we set r_k to the expected value of the distance to the k th nearest point in a PPP: $r_k = \frac{\Gamma(k+1.5)}{\sqrt{\pi\lambda_b} \Gamma(k+1)}$ for $k = 1, \dots, 100$ [47]. We further set $\eta = 3.8$ and $\lambda_b = 2$ BSs/km² and neglect the noise. Shown in Fig. 1 is $C(\rho)$ in (15) compared against C_{exact} . The same comparison is provided for MIMO with $N_t = N_r = 2$. In both cases the differences are minute, supporting the interference modeling approach propounded in this paper.

IV. DISTRIBUTION OF THE LOCAL-AVERAGE SINR

Thus far, the BS locations $\{r_k\}$ have been conditioned upon. Once they are released, ρ becomes itself a random variable whose distribution is induced by the process Φ_b . The corresponding CDF, $F_\rho(\cdot)$, is to be a central ingredient in our analysis of the ergodic spectral efficiency. This important function, extensively utilized by system designers, has traditionally been obtained by means of simulation over lattice networks with shadowing and random translations [48]. For hexagonal cells in particular, and without shadow fading, an infinite series solution is also available [49].

Here we set out to characterize $F_\rho(\cdot)$ for Poisson networks, so as to implicitly incorporate shadowing, and specifically for interference-limited Poisson networks. Interestingly, with PPP-populated BSs, the powers received by any given user are statistically invariant—save for a scaling of the BS density if noise were not negligible—to the distribution of the channel gains [32]–[34] and thus $F_\rho(\cdot)$ is equivalent to what $F_{\text{SIR}}(\cdot)$ would look like if users connected to the BS with the strongest instantaneous link. This distribution was established in [14], [50]–[52], very compactly for arguments above 1 and in a still manageable form for arguments between 1/2 and 1, but in an accelerating cumbersome fashion (involving progressively higher-dimensional integrations) as the argument of the CDF dips below 1/2 [51, Sec. V.A], [52, Cor. 19]. As alternatives, [19], [50], [53] derived $F_{1/\rho}(\cdot)$ in the Laplace domain, which would then require numerical inversion, while [54] showed that the lower tail ($\theta \rightarrow 0$) of $F_\rho(\theta)$ satisfies

$$\log F_\rho(\theta) = \frac{s^*}{\theta} + o(1) \quad (17)$$

with $s^* < 0$ being the solution to

$$s^{*\delta} \bar{\Gamma}(-\delta, s^*) = 0 \quad (18)$$

where $\bar{\Gamma}$ is the lower incomplete gamma function and, for compactness, we have introduced the shorthand notation $\delta = 2/\eta$. Since it only depends—through δ —on the path loss exponent η , the parameter s^* can be precomputed for all relevant values thereof by solving (18) using any standard software package. Values of s^* for some typical η are listed in Table I.

The approach we take is to apply the exact form down to $\theta = 1/2$ and then (17) for $\theta < 1/2$.

TABLE I: Parameter s^* and the corresponding δ for typical values of the path loss exponent η .

η	δ	s^*									
3.5	0.571	-0.672	3.7	0.540	-0.747	3.9	0.513	-0.819	4.1	0.488	-0.888
3.6	0.556	-0.71	3.8	0.526	-0.783	4	0.5	-0.854	4.2	0.476	-0.922

This combination gives

$$\left\{ \begin{array}{ll} F_\rho(\theta) \simeq e^{s^*/\theta} & 0 \leq \theta < \frac{s^*}{\log A_\delta} \\ F_\rho(\theta) \approx A_\delta & \frac{s^*}{\log A_\delta} \leq \theta < 1/2 \\ F_\rho(\theta) = 1 - \theta^{-\delta} \text{sinc } \delta + B_\delta\left(\frac{\theta}{1-\theta}\right) & 1/2 \leq \theta < 1 \\ F_\rho(\theta) = 1 - \theta^{-\delta} \text{sinc } \delta & \theta \geq 1, \end{array} \right. \quad (19)$$

where " \simeq " indicates an approximation with asymptotic ($\theta \rightarrow 0$) equality while

$$A_\delta = 1 - 2^\delta \text{sinc } \delta + B_\delta(1) \quad (20)$$

and

$$B_\delta(x) = \frac{\delta \text{sinc}^2(\delta) \Gamma^2(\delta + 1) {}_2F_1(1, \delta + 1; 2\delta + 2; -1/x)}{x^{1+2\delta} \Gamma(2\delta + 2)} \quad (21)$$

with ${}_2F_1$ the Gauss hypergeometric function. When the path loss exponent is $\eta = 4$, we have that $\delta = 1/2$ and the above specialize to

$$\left\{ \begin{array}{ll} F_\rho(\theta) \simeq e^{-0.854/\theta} & 0 \leq \theta < 0.457 \\ F_\rho(\theta) \approx 0.154 & 0.457 \leq \theta < 1/2 \\ F_\rho(\theta) = 1 - \frac{4\sqrt{\theta}-\theta-1}{\pi\theta} & 1/2 \leq \theta < 1 \\ F_\rho(\theta) = 1 - \frac{2}{\pi\sqrt{\theta}} & \theta \geq 1. \end{array} \right. \quad (22)$$

An even simpler, slightly less accurate expression for $F_\rho(\cdot)$ is obtained using the exact form only down to $\theta = 1$ while stretching the lower tail expansion in (17) up to $\theta = 1$. This gives

$$\left\{ \begin{array}{ll} F_\rho(\theta) \simeq e^{s^*/\theta} & 0 \leq \theta < \frac{s^*}{\log(1-\text{sinc } \delta)} \\ F_\rho(\theta) \approx 1 - \text{sinc } \delta & \frac{s^*}{\log(1-\text{sinc } \delta)} \leq \theta < 1 \\ F_\rho(\theta) = 1 - \theta^{-\delta} \text{sinc } \delta & \theta \geq 1. \end{array} \right. \quad (23)$$

V. DISTRIBUTION OF THE SPECTRAL EFFICIENCY

The randomness that ρ acquires once the BS positions are randomized is then inherited by C , and the corresponding CDF provides a complete description of the ergodic spectral efficiency offered by the network over all locations [8]. By mapping the applicable function $C(\rho)$ onto the expressions for $F_\rho(\cdot)$ put forth in the previous section, $F_C(\cdot)$ is readily characterized. In interference-limited conditions, such $F_C(\cdot)$ depends only on the path loss exponent, η .

A. SISO

In Rayleigh-faded SISO channels, $C(\rho)$ is given by (15). By resorting to the invertible approximation [55]

$$e^\nu E_1(\nu) \log_2 e \approx 1.4 \log \left(1 + \frac{0.82}{\nu} \right) \quad (24)$$

it becomes possible to write $\rho \approx \frac{e^{C/1.4}-1}{0.82}$ and subsequently, by means of (19),

$$F_C(\gamma) \approx F_\rho \left(\frac{e^{\frac{\gamma}{1.4}} - 1}{0.82} \right) \quad (25)$$

$$= \begin{cases} e^{\frac{0.82 s^*}{\exp(\gamma/1.4)-1}} & 0 \leq \gamma < 1.4 \log \left(1 + \frac{0.82 s^*}{\log A_\delta} \right) \\ A_\delta & 1.4 \log \left(1 + \frac{0.82 s^*}{\log A_\delta} \right) \leq \gamma < 0.48 \\ 1 - \frac{\text{sinc } \delta}{\left(\frac{e^{\gamma/1.4}-1}{0.82} \right)^\delta} + B_\delta \left(\frac{e^{\gamma/1.4}-1}{1.82-e^{\gamma/1.4}} \right) & 0.48 \leq \gamma < 0.84 \\ 1 - \frac{\text{sinc } \delta}{\left(\frac{e^{\gamma/1.4}-1}{0.82} \right)^\delta} & \gamma \geq 0.84, \end{cases} \quad (26)$$

whose accuracy is validated in the following example.

Example 4. Consider an interference-limited network with $\eta = 3.8$. Shown in Fig. 2 are (26), as well as the numerical mapping of $C(\rho)$ —without the bypass of its invertible approximation—onto (19), both solutions contrasted against C_{exact} . For the computation of C_{exact} via Monte-Carlo, here and in all examples involving simulations hereafter, PPP-populated BSs (1000 on average) are dropped in a disk centered at the receiver.

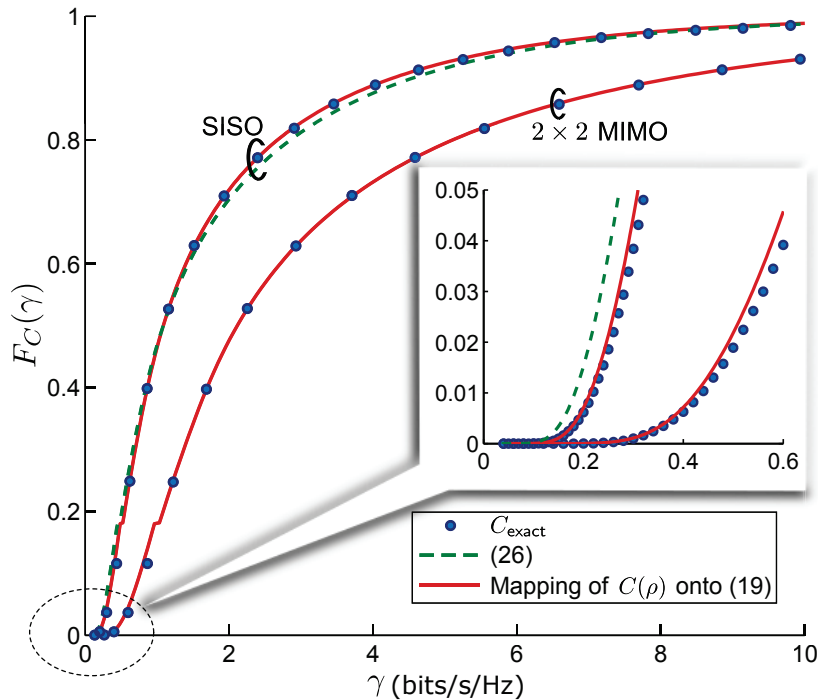


Fig. 2: CDF of ergodic spectral efficiency for $\eta = 3.8$. In the inset, a zoom-in of the lower tail.

For $\eta = 4$, (26) specializes to

$$F_C(\gamma) \approx \begin{cases} e^{-\frac{0.7}{\exp(\gamma/1.4)-1}} & 0 \leq \gamma < 0.44 \\ 0.154 & 0.44 \leq \gamma < 0.48 \\ 1 - \frac{4}{\pi} \sqrt{\frac{0.82}{e^{\gamma/1.4}-1}} + \frac{e^{\gamma/1.4}-0.18}{\pi(e^{\gamma/1.4}-1)} & 0.48 \leq \gamma < 0.84 \\ 1 - \frac{2}{\pi} \sqrt{\frac{0.82}{e^{\gamma/1.4}-1}} & \gamma \geq 0.84. \end{cases} \quad (27)$$

In contrast to these pleasing results, without the model for z propounded in this paper the distribution of the spectral efficiency over the network locations is far more inaccessible. Indeed, the corresponding C_{ub} can be rewritten (cf. Appendix B) as

$$C_{\text{ub}} = \log_2 e \int_0^\infty \frac{e^{-x r_0^\eta N_0/P}}{1+x} \prod_{k=1}^\infty \frac{1}{1+x(r_0/r_k)^\eta} dx, \quad (28)$$

which is no longer a function of singly ρ , whose distribution was established in the previous section; rather, (28) is a more involved function of $\{r_k\}_{k=0}^\infty$ and offers no obvious way of disentangling these dependences. Faced with this obstacle, some authors choose to instead characterize the distribution of $\log_2 \left(1 + \frac{P r_0^{-\eta} |H_0|^2}{P \sum_{k=1}^\infty r_k^{-\eta} |H_k|^2 + N_0} \right)$ over $\{H_k\}_{k=0}^\infty$ as well as $\{r_k\}_{k=0}^\infty$ [56] [57, Sec. VII.A]. However, the mixing of small- and large-scale variations within this

quantity clutters potential observations. Moreover, the generalization to more involved settings, say MIMO, appears arduous or outright hopeless. Indeed, existing stochastic geometry analyses of spectral efficiency featuring MIMO are restricted to beamforming or space-division multiple access, rather than spatial multiplexing [22]–[26], [56].

B. MIMO

Our approach, in contrast, only requires mapping the appropriate $C(\rho)$ onto $F_\rho(\cdot)$. Whenever $C(\rho)$ does not lend itself to inversion, even approximately, it is straightforward to perform this mapping numerically.

Example 5. Reconsider Example 4, but now with $N_t = N_r = 2$ such that, from (16),

$$C_{2 \times 2}^{\text{MIMO}}(\rho) = 2 e^{2/\rho} \left[E_1\left(\frac{2}{\rho}\right) + E_3\left(\frac{2}{\rho}\right) \right] \log_2 e \quad (29)$$

$$= \left[2 e^{2/\rho} E_1\left(\frac{2}{\rho}\right) \left(1 + \frac{2}{\rho^2}\right) + \left(1 - \frac{2}{\rho}\right) \right] \log_2 e. \quad (30)$$

Fig. 2 depicts the numerical mapping of $C_{2 \times 2}^{\text{MIMO}}(\rho)$ onto (19), as well as the corresponding C_{exact} .

C. Lognormal Fit

Inspecting the distribution of $C(\rho)$ we observe that, interestingly, it closely resembles a lognormal function, i.e., that $\log C(\rho)$ admits a rather precise Gaussian fit. This opens the door to an alternative to $F_C(\cdot)$ as obtained by mapping $C(\rho)$ onto $F_\rho(\cdot)$, namely the alternative $\log C(\rho) \sim \mathcal{N}(\mu, \sigma^2)$ with

$$\mu = \int_0^\infty \log C(\theta) dF_\rho(\theta) \quad (31)$$

$$\sigma^2 = \int_0^\infty [\log C(\theta)]^2 dF_\rho(\theta) - \mu^2. \quad (32)$$

Example 6. Let $\eta = 4$. For $C_{2 \times 2}^{\text{MIMO}}(\rho)$ as given in (30) and $F_\rho(\cdot)$ as given in (22), the numerical integrations in (31)–(32) yield $\mu = 0.92$ and $\sigma^2 = 0.8$. Fig. 3 presents the empirical PDF of $\log C_{2 \times 2}^{\text{MIMO}}(\rho)$, generated via Monte-Carlo, and a Gaussian PDF with $\mu = 0.92$ and $\sigma^2 = 0.8$.

Thanks to this lognormal behavior, which holds for both SISO and MIMO, a Gaussian distribution with mean μ and variance σ^2 can provide a quick idea of the disparity of the user experiences throughout the network. This complements the coverage analysis presented in

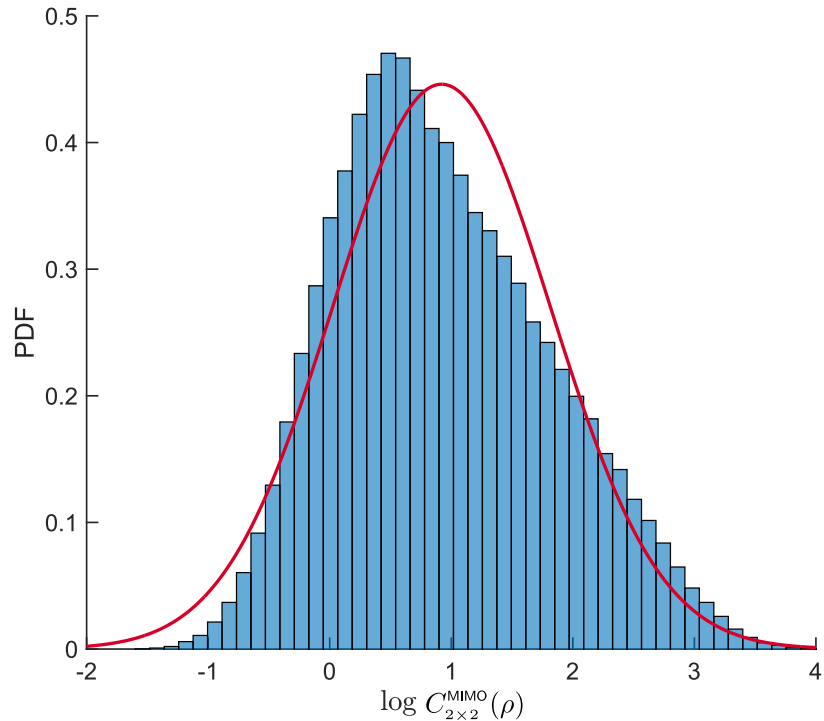


Fig. 3: Empirical PDF of the logarithm of the 2×2 MIMO ergodic spectral efficiency for $\eta = 4$ and its normal fit.

the next section, which is more precise but valid only for the lower tail. The lognormal fit, rather, may be used to determine the fraction of users whose spectral efficiency lies within a certain interval of the average, or it may simplify further calculations that require averaging with respect to the distribution of $C(\rho)$.

VI. COVERAGE

While the entire CDF of ergodic spectral efficiency is relevant from a network-design perspective, the lower tail is especially important as it determines the coverage, i.e., the share of network locations in which a minimum level of service can be provided. The shape of the lower tail, in particular, reveals the improvement in coverage with a diminishing service requirement or, equivalently, the sacrifice in coverage that is necessary to guarantee a better minimum service. The behavior of this tail (which, for $\eta = 3.8$, is detailed in the inset of Fig. 2) warrants attention, and this section is devoted precisely to its analysis and to gleaning coverage insights from it.

A. SISO

For SISO, the CDF lower tail is seen from (25) to behave as

$$F_C(\gamma) \approx e^{\frac{0.82 s^*}{\exp(\gamma/1.4)-1}}. \quad (33)$$

Using $e^{\gamma/1.4} - 1 = 0.72\gamma + \mathcal{O}(\gamma^2)$, the tail behavior can be re-expressed as

$$F_C(\gamma) \approx e^{1.15 s^*/\gamma} \quad (34)$$

where, recall, s^* is negative. By inverting (34), the spectral efficiency γ achievable on a share $1 - \xi$ of the network is seen to satisfy (for $\xi \leq A_\delta$)

$$\gamma \approx \frac{1.15 s^*}{\log_e \xi}. \quad (35)$$

For $\eta = 4$, we can recall $s^* = -0.854$ and the above direct and inverse expressions then specialize, respectively, to

$$F_C(\gamma) \approx e^{-1/\gamma} \quad (36)$$

and (for $\xi \leq 0.154$)

$$\gamma \approx \frac{1}{\log_e 1/\xi}. \quad (37)$$

Example 7. For SISO and $\eta = 4$, (36) is depicted in Fig. 4 alongside previously obtained expressions for $F_C(\cdot)$ as well as the exact tail computed via Monte-Carlo.

Example 8. For SISO and $\eta = 4$, the spectral efficiency γ achievable in 99% of the network satisfies

$$\gamma \approx \frac{1}{\log_e 100} = 0.22 \quad (38)$$

whereas the exact value, obtained numerically, equals 0.24 bits/s/Hz.

B. MIMO

With N_t transmit and N_r receive antennas, the ergodic capacity expands as [58]

$$C(\rho) = N_r \rho \log_2 e + \mathcal{O}(\rho^2) \quad (39)$$

indicating a linear scaling with N_r and no dependence on N_t . This low-SNR behavior is very robust, holding irrespectively of the fading distribution and in the face of antenna correlation, signifying that what matters in this regime is only the receiver's ability to capture power.

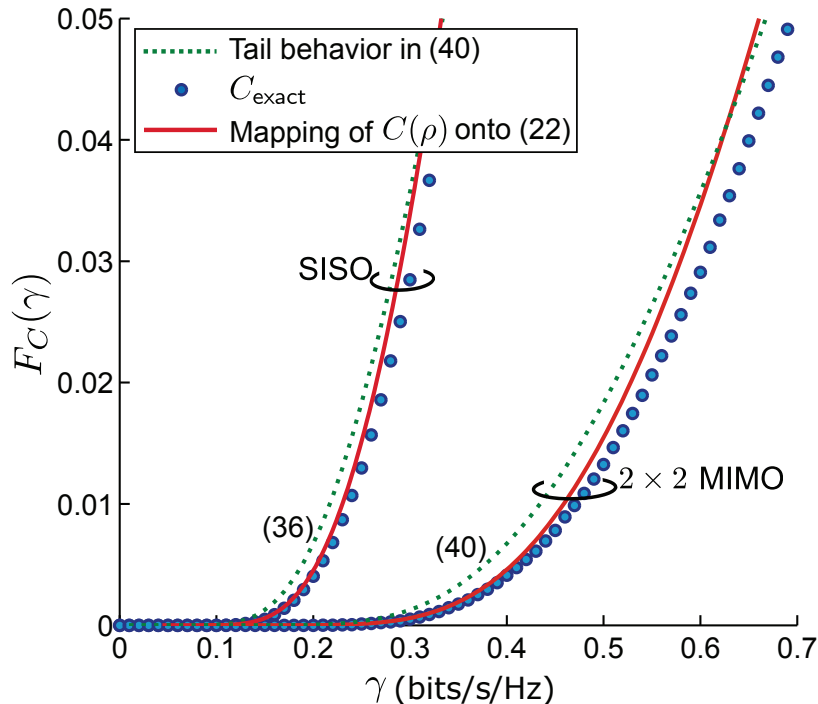


Fig. 4: Lower tail of the ergodic spectral efficiency CDF for $\eta = 4$.

Applying the linear scaling of the low-SNR capacity with N_r to (34) and (35) we obtain

$$F_C(\gamma) \approx e^{1.15 s^* N_r / \gamma} \quad (40)$$

and

$$\gamma \approx \frac{1.15 s^* N_r}{\log_e \xi}. \quad (41)$$

which can be readily specialized to $\eta = 4$ as well.

Example 9. For $N_t = N_r = 2$ and $\eta = 4$, (40) is depicted in Fig. 4 alongside previously obtained expressions for $F_C(\cdot)$ as well as the exact tail computed via Monte-Carlo.

Since coverage is not gained or lost in reference to small-scale fades, which are highly localized in space, time and frequency, care must be exercised not to infer coverage from the distribution of instantaneous SINR or of instantaneous spectral efficiency, both of which are dominated by small-scale fading. With Rayleigh fading and $\eta = 4$ in particular, the distribution of the instantaneous SIR throughout the network equals [1]

$$F_{\text{SIR}}(\theta) = 1 - \frac{1}{1 + \sqrt{\theta} \arctan(\sqrt{\theta})} \quad (42)$$

whose lower tail behaves as $F_{\text{SIR}}(\theta) = \theta + \mathcal{O}(\theta^2)$. This linear decay is drastically different from the exponential ones derived in this section on the basis of $F_C(\cdot)$. At 99% coverage, $F_{\text{SIR}}(\cdot)$ would map to a value of 0.014 bits/s/Hz, far from the exact value of 0.24 and from the value of 0.22 we obtained in Example 8. It is therefore important that coverage be gleaned from the ergodic spectral efficiency, which is impervious to small-scale fluctuations, rather than from quantities subject to those fluctuations.

VII. SPATIAL AVERAGE OF THE SPECTRAL EFFICIENCY

Sometimes, it is of interest to condense $F_C(\cdot)$ down to a single quantity, and in that case the average is the logical choice. Under spatial ergodicity, which holds for the PPP and many other point processes [9], this quantity equals the average of all per-user spectral efficiencies in any realization of the network.

Here again, the approach propounded in this paper proves advantageous. For any setting for which $C(\rho)$ is available, our expressions for $F_\rho(\cdot)$ enable computing

$$\bar{C} = \int_0^\infty C(\theta) dF_\rho(\theta), \quad (43)$$

which, in interference-limited conditions, again depends only on the path loss exponent. Remarkably, the above integration can be solved for SISO and for (at least some) MIMO settings, and the expressions obtained involve only readily computable special functions. Although devoid of insight, these expressions allow circumventing large-scale Monte-Carlo simulations.

A. SISO

In Rayleigh-faded SISO channels, with (15) and (23) plugged into (43), the integration yields (cf. Appendix C)

$$\bar{C} \approx \frac{-s^* \log_2 e}{1 + s^*} \left[E_1(-s^*/D_\delta) - e^{(1+s^*)/D_\delta} E_1(1/D_\delta) \right] + \frac{\sin(\pi\delta) \log_2 e}{\pi} G_{2,3}^{2,2} \left(1 \left| \begin{array}{l} 0, 1 - \delta \\ 0, 0, -\delta \end{array} \right. \right) \quad (44)$$

where

$$G_{p,q}^{m,n} \left(z \left| \begin{array}{l} a_1, \dots, a_n, a_{n+1}, \dots, a_p \\ b_1, \dots, b_m, b_{m+1}, \dots, b_q \end{array} \right. \right) \quad (45)$$

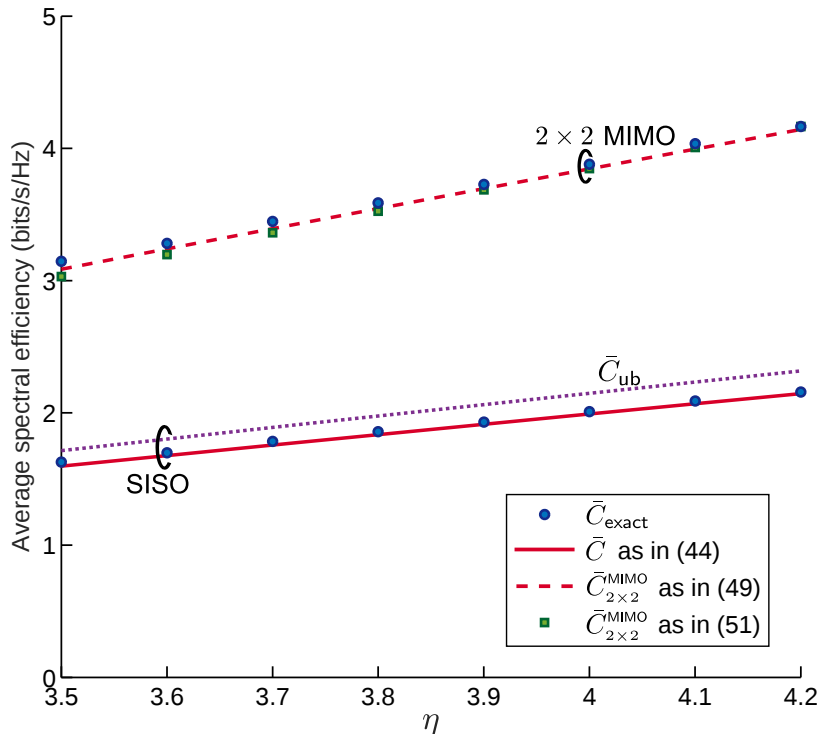


Fig. 5: Spatially averaged ergodic spectral efficiency as a function of η for SISO and for 2×2 MIMO. The 99% confidence interval around the Monte-Carlo results ranges from ± 0.008 at $\eta = 3.5$ to ± 0.01 at $\eta = 4.2$ for SISO and from ± 0.015 at $\eta = 3.5$ to ± 0.02 at $\eta = 4.2$ for MIMO. The SISO upper bound \bar{C}_{ub} is computed via (48).

is the Meijer-G function while $D_\delta = s^*/\log(1 - \text{sinc } \delta)$. An even more precise, albeit also more involved expression for \bar{C} can be obtained using (19) in lieu of (23).

Example 10. Fig. 5 compares (44) against \bar{C}_{exact} , the Monte-Carlo average of C_{exact} , for $0.48 \leq \delta \leq 0.57$ corresponding to $3.5 \leq \eta \leq 4.2$. For $\eta = 4$ in particular,

$$\bar{C} \approx 0.187 + \frac{\log_2 e}{\pi} G_{2,3}^{2,2} \left(1 \left| \begin{matrix} 0, 1/2 \\ 0, 0, -1/2 \end{matrix} \right. \right) = 1.99, \quad (46)$$

while \bar{C}_{exact} is 2.01

It is worthwhile to contrast (44) with its counterpart obtained without the model for z propounded in this paper, namely the average of C_{ub} given by [1]

$$\bar{C}_{\text{ub}} = \int_0^\infty \frac{\log_2 e}{1 + (e^t - 1)^\delta} \int_{(e^t - 1)^{-\delta}}^\infty \frac{1}{1 + x^{1/\delta}} dx dt, \quad (47)$$

or, by means of Pfaff's transformation [59], equivalently by

$$\bar{C}_{\text{ub}} = \int_0^\infty \frac{\log_2 e}{{}_2F_1\left(1, 1; 1 - \delta; \frac{\gamma}{1+\gamma}\right)} d\gamma. \quad (48)$$

Example 11. Included in Fig. 5, alongside its SISO counterparts \bar{C} and \bar{C}_{exact} , is also \bar{C}_{ub} .

Besides being further from C_{exact} than our solution \bar{C} , and requiring either a double integration or a single integral over a hypergeometric function, neither of the expressions for \bar{C}_{ub} offers a viable path to MIMO generalization. With our approach, in contrast, the analysis of the spatial average becomes feasible also with MIMO.

B. MIMO

For 2×2 MIMO, the integration of $C_{2 \times 2}^{\text{MIMO}}(\rho)$ as given in (30) over $F_\rho(\cdot)$ as given in (23) returns (cf. Appendix C)

$$\begin{aligned} \bar{C}_{2 \times 2}^{\text{MIMO}} \approx & \frac{2s^* e^{\frac{2+s^*}{D_\delta}} \left[2(2+s^*)^2 - 4(2+s^*)D_\delta + (8+s^*(4+s^*))D_\delta^2 \right] E_1(2/D_\delta)}{(2+s^*)^3 D_\delta^2 \log 2} \\ & + \frac{s^* D_\delta \left[2(8+s^*(4+s^*))D_\delta E_1(-s^*/D_\delta) - e^{s^*/D_\delta} (2+s^*) \left((6+s^*)D_\delta - 2(2+s^*) \right) \right]}{(2+s^*)^3 D_\delta^2 \log 2} \\ & + \frac{\sin(\pi\delta) \log_2 e}{\pi} \left[2 G_{2,3}^{2,2} \left(1 \left| \begin{matrix} 0, 1 - \delta \\ 0, 0, -\delta \end{matrix} \right. \right) + 4 G_{2,3}^{2,2} \left(1 \left| \begin{matrix} 0, -1 - \delta \\ 0, 0, -2 - \delta \end{matrix} \right. \right) + \frac{1 - \delta}{(1 + \delta)\delta} \right]. \end{aligned} \quad (49)$$

An alternative expression not involving the Meijer-G function can be obtained using $E_3(x) \approx \frac{e^{-3x/2}}{2}$ and $2e^{\frac{2}{\rho}} E_1\left(\frac{2}{\rho}\right) \log_2 e \approx 2.8 \log(1 + 0.41 \rho)$ to simplify $C_{2 \times 2}^{\text{MIMO}}(\rho)$ in (29) into

$$C_{2 \times 2}^{\text{MIMO}}(\rho) \approx 2.8 \log(1 + 0.41 \rho) + e^{-1/\rho} \log_2 e. \quad (50)$$

Using this form in place of (30) in the integration (cf. Appendix C),

$$\begin{aligned} \bar{C}_{2 \times 2}^{\text{MIMO}} \approx & \frac{s^* \log_2 e}{(s^* - 1) e^{(s^*-1)/D_\delta}} + \delta \text{sinc}(\delta) \bar{\Gamma}(\delta, 1) \log_2 e \\ & + 2.8 \left[e^{-0.41 s^*} E_1(-s^*(0.41 + 1/D_\delta)) - E_1(-s^*/D_\delta) + e^{s^*/D_\delta} \log(1 + 0.41 D_\delta) \right] \\ & + 2.8 \left[{}_2F_1(1, \delta, 1 + \delta, -2.44) + \delta \log(1.41) \right] \frac{\text{sinc}(\delta)}{\delta}. \end{aligned} \quad (51)$$

Example 12. Fig. 5 compares (49) and (51) against \bar{C}_{exact} . For $\eta = 4$ in particular, (51) returns

$$\bar{C}_{2 \times 2}^{\text{MIMO}} \approx 0.26 + \frac{\log_2 e}{\sqrt{\pi}} \text{erf}(1) + \frac{5.6}{\pi} \left[\sqrt{0.41} \left(\pi - 2 \arctan(\sqrt{0.41}) \right) + \log 1.41 \right] = 3.84 \quad (52)$$

TABLE II: Spatially averaged ergodic spectral efficiency $\bar{C}_{N_r \times N_t}^{\text{MIMO}}$ with $\eta = 4$.

$N_t \backslash N_r$	1	2	3	4
1	1.99	2.76	3.25	3.62
2	2.13	3.84	4.79	5.48
3	2.18	4.11	5.71	6.75
4	2.21	4.24	6.05	7.59

while the Monte-Carlo average of its C_{exact} counterpart is 3.87.

Combining Examples 10 and 12, two-antenna single-user MIMO is seen from our analysis to provide a 93% increase in the spectral efficiency of an entire interference-limited network, a determination that would classically have entailed very extensive simulations.

For higher-order MIMO, the integration of $C_{N_r \times N_t}^{\text{MIMO}}(\rho)$ over $F_\rho(\cdot)$ in (23) yields the single-integral solution

$$\bar{C}_{N_r \times N_t}^{\text{MIMO}} \approx \log_2 e \sum_{i=0}^{m-1} \sum_{j=0}^i \sum_{\ell=0}^{2j} \left\{ \binom{2i-2j}{i-j} \binom{2j+2n-2m}{2j-\ell} \frac{(-1)^\ell (2j)! (n-m+\ell)!}{2^{2i-\ell} j! \ell! (n-m+j)!} \cdot \sum_{q=0}^{n-m+\ell} \int_0^\infty \frac{1}{(1+\gamma)^{q+1}} \left[\frac{s^*}{s^* - \gamma N_t} e^{\frac{s^* - \gamma N_t}{D\delta}} + \delta \text{sinc}(\delta) \frac{\bar{\Gamma}(\delta, \gamma N_t)}{(\gamma N_t)^\delta} \right] d\gamma \right\}. \quad (53)$$

Although, for some antenna configurations beyond $N_t = N_r = 2$, it may be possible to express this integral via special functions, it is beside the point once the expressions become overly intricate. Rather, it seems preferable to directly integrate numerically for each specific path loss exponent of interest.

Example 13. Shown in Table II is $\bar{C}_{N_r \times N_t}^{\text{MIMO}}$ computed via (53) for different values of N_t and N_r with the path loss exponent $\eta = 4$.

VIII. SECTORIZATION

Let us now incorporate cell sectorization to the model. Each BS, now allowed to comprise S sector antennas uniformly staggered in azimuth, communicates with one user per channel and per sector (cf. Fig. 6). From the vantage of the user at the origin, the downlink signals from the sectors of any given BS undergo the same path loss and shadowing but different antenna gains.

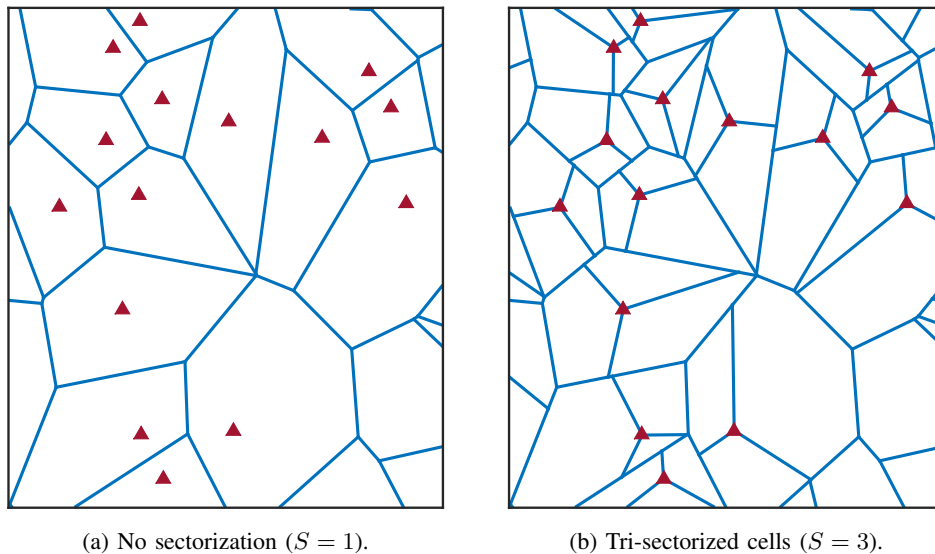


Fig. 6: Tesselation of a Poisson network, with and without sectorization.

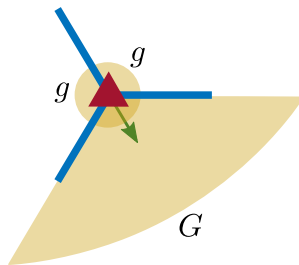


Fig. 7: Antenna pattern for $S = 3$ with in-sector gain G and out-of-sector gain g .

Given an arbitrary azimuth pattern for the sector antennas, [19] characterized the local-average SINR distribution in the Laplace domain. Differently, we provide direct expressions that rely only on the antenna front-to-back ratio $Q \geq 1$ and on the number of sectors, S . Given an in-sector gain $G = \frac{QS}{Q+S-1}$ and an out-of-sector gain $g = \frac{S}{Q+S-1}$, our model for the antenna pattern as a function of the azimuth ϕ is (cf. Fig. 7)

$$g_s(\phi) = \begin{cases} G & \phi_0 - \pi/S \leq \phi < \phi_0 + \pi/S \\ g & \text{elsewhere,} \end{cases} \quad (54)$$

where ϕ_0 indicates the orientation of the antenna. This way, it is ensured that the total radiated

power is preserved, i.e., that

$$\int_0^{2\pi} \frac{g_s(\phi)}{2\pi} d\phi = 1. \quad (55)$$

Setting $S = 1$ we recover an unsectorized network where $g_1(\phi) = 1$. In turn, for $Q \rightarrow \infty$, the S sectors become ideal as $G \rightarrow S$ and $g \rightarrow 0$. Under the foregoing model, the intended signal from the serving sector has gain G while the $(S - 1)$ interfering transmissions from other sectors of the same BS have gain g . The S transmissions from every other BS add to the interference.

The small-scale fading in the link from each sector is independent and of unit-power, with the receiver knowing only the fading experienced by the intended signal.

A. Local-Average SINR

With P now denoting the per-sector transmit power, the total power that each interfering BS launches towards the user at the origin is $P(G + (S - 1)g) = PS$. Since the useful signal launched by the intended BS is PG , the local-average SINR at the origin is

$$\rho_s = \frac{PG r_0^{-\eta}}{P(S - 1)g r_0^{-\eta} + PS \sum_{k=1}^{\infty} r_k^{-\eta} + N_0}, \quad (56)$$

irrespective of how the sectors are oriented at each BS. (This orientation-invariance is not an artifact of our model; rather, it has been shown that the distribution of ρ_s is insensitive to the sector orientations regardless of the antenna patterns [19].)

In interference-limited conditions, the local-average SINR becomes

$$\rho_s = \frac{Q r_0^{-\eta}}{(S - 1) r_0^{-\eta} + (Q + S - 1) \sum_{k=1}^{\infty} r_k^{-\eta}}, \quad (57)$$

which, with ideal sectorization, i.e., for $Q \rightarrow \infty$, converges to its unsectorized self, $\rho = r_0^{-\eta} / \sum_{k=1}^{\infty} r_k^{-\eta}$. It follows that, under ideal sectorization, all the results derived for unsectorized networks continue to apply, only on a per-sector rather than a per-BS basis. Conversely, under nonideal sectors, the CDF of ρ_s can be obtained as

$$\begin{aligned} F_{\rho_s}(\theta) &= \mathbb{P} \left[\frac{Q r_0^{-\eta}}{(S - 1) r_0^{-\eta} + (Q + S - 1) \sum_{k=1}^{\infty} r_k^{-\eta}} < \theta \right] = \mathbb{P} \left[\frac{r_0^{-\eta}}{\sum_{k=1}^{\infty} r_k^{-\eta}} < \frac{Q + S - 1}{Q/\theta - S + 1} \right] \\ &= \begin{cases} F_{\rho} \left[\frac{Q + S - 1}{Q/\theta - S + 1} \right] & 0 \leq \theta < \frac{Q}{S - 1} \\ 1 & \theta \geq \frac{Q}{S - 1}, \end{cases} \end{aligned} \quad (58)$$

which is capped at $\frac{Q}{S-1}$ because of interference among same-BS sectors. Plugging (19) into (58),

$$\left\{ \begin{array}{l} F_{\rho_S}(\theta) \simeq e^{s^* \frac{Q/\theta - S + 1}{Q + S - 1}} \\ F_{\rho_S}(\theta) \approx A_\delta \\ F_{\rho_S}(\theta) = 1 - \frac{\text{sinc } \delta}{\left(\frac{Q + S - 1}{Q/\theta - S + 1}\right)^\delta} + B_\delta \left[\frac{Q + S - 1}{Q(1/\theta - 1) - 2(S - 1)} \right] \\ F_{\rho_S}(\theta) = 1 - \frac{\text{sinc } \delta}{\left(\frac{Q + S - 1}{Q/\theta - S + 1}\right)^\delta} \\ F_{\rho_S}(\theta) = 1 \end{array} \right. \quad \begin{array}{l} 0 \leq \theta < \frac{s^* Q / \log A_\delta}{Q + (1 + s^* / \log A_\delta)(S - 1)} \\ \frac{s^* Q / \log A_\delta}{Q + (1 + s^* / \log A_\delta)(S - 1)} \leq \theta < \frac{Q}{2Q + 3(S - 1)} \\ \frac{Q}{2Q + 3(S - 1)} \leq \theta < \frac{Q}{Q + 2(S - 1)} \\ \frac{Q}{Q + 2(S - 1)} \leq \theta < \frac{Q}{S - 1} \\ \theta \geq \frac{Q}{S - 1}, \end{array} \quad (59)$$

which, for $\eta = 4$, specializes to

$$\left\{ \begin{array}{l} F_{\rho_S}(\theta) \simeq e^{-0.854 \frac{Q/\theta - S + 1}{Q + S - 1}} \\ F_{\rho_S}(\theta) \approx 0.154 \\ F_{\rho_S}(\theta) = 1 - \frac{4}{\pi} \sqrt{\frac{Q/\theta - S + 1}{Q + S - 1}} + \frac{Q}{\pi} \frac{1 + 1/\theta}{Q + S - 1} \\ F_{\rho_S}(\theta) = 1 - \frac{2}{\pi} \sqrt{\frac{Q/\theta - S + 1}{Q + S - 1}} \\ F_{\rho_S}(\theta) = 1 \end{array} \right. \quad \begin{array}{l} 0 \leq \theta < \frac{0.457 Q}{Q + 1.457(S - 1)} \\ \frac{0.457 Q}{Q + 1.457(S - 1)} \leq \theta < \frac{Q}{2Q + 3(S - 1)} \\ \frac{Q}{2Q + 3(S - 1)} \leq \theta < \frac{Q}{Q + 2(S - 1)} \\ \frac{Q}{Q + 2(S - 1)} \leq \theta < \frac{Q}{S - 1} \\ \theta \geq \frac{Q}{S - 1}. \end{array} \quad (60)$$

Alternatively, plugging (23) into (58), a simpler and slightly less accurate expression is obtained, precisely

$$\left\{ \begin{array}{l} F_{\rho_S}(\theta) \simeq e^{s^* \frac{Q/\theta - S + 1}{Q + S - 1}} \\ F_{\rho_S}(\theta) \approx 1 - \text{sinc } \delta \\ F_{\rho_S}(\theta) = 1 - \frac{\text{sinc } \delta}{\left(\frac{Q + S - 1}{Q/\theta - S + 1}\right)^\delta} \\ F_{\rho_S}(\theta) = 1 \end{array} \right. \quad \begin{array}{l} 0 \leq \theta < \frac{s^* Q / \log(1 - \text{sinc } \delta)}{Q + [1 + s^* / \log(1 - \text{sinc } \delta)](S - 1)} \\ \frac{s^* Q / \log(1 - \text{sinc } \delta)}{Q + [1 + s^* / \log(1 - \text{sinc } \delta)](S - 1)} \leq \theta < \frac{Q}{Q + 2(S - 1)} \\ \frac{Q}{Q + 2(S - 1)} \leq \theta < \frac{Q}{S - 1} \\ \theta \geq \frac{Q}{S - 1}. \end{array} \quad (61)$$

Example 14. Let $\eta = 4$. Shown in Fig. 8 are $F_\rho(\cdot)$ without sectorization and $F_{\rho_3}(\cdot)$ with $Q = 20$ dB, which is a rather typical front-to-back ratio.

Although, as Fig. 8 visualizes, nonideal sectorization puts a hard ceiling on the SIR, this only affects the distribution modestly. In exchange, the available bandwidth gets to be reused S times per cell and thus sectorization is decidedly advantageous.

B. Ergodic Spectral Efficiency

As in Section V, the CDF of the ergodic spectral efficiency $F_C(\cdot)$ is characterized by mapping the applicable function $C(\rho_S)$ onto $F_{\rho_S}(\cdot)$. For Rayleigh-faded SISO channels in particular, we

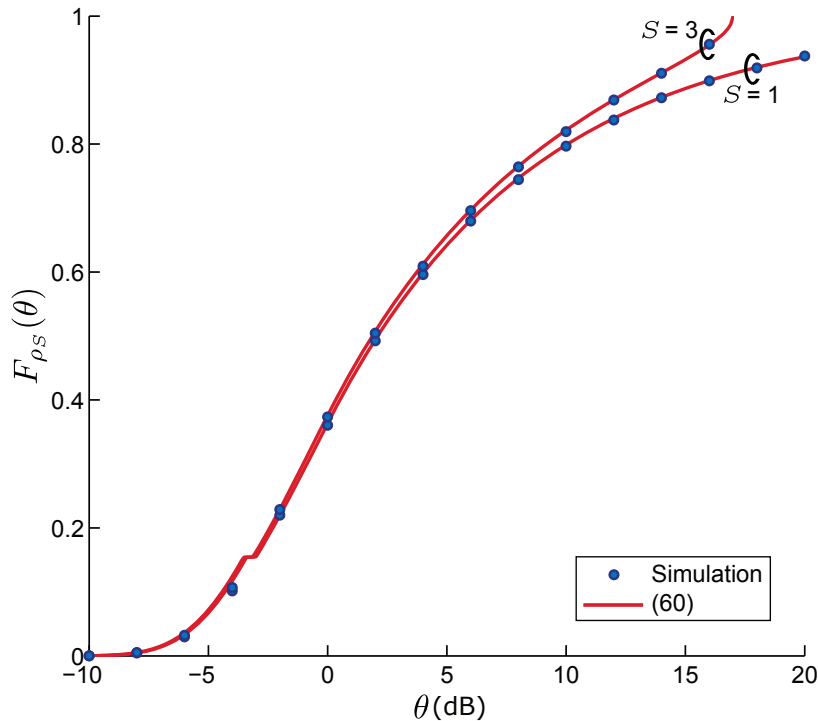


Fig. 8: $F_{\rho}(\cdot)$ without sectorization and $F_{\rho_3}(\cdot)$ with $Q = 20$ dB, both for $\eta = 4$.

can invoke (25) to explicitly express this mapping as

$$F_C(\gamma) \approx F_{\rho_S} \left(\frac{e^{\frac{\gamma}{1.4}} - 1}{0.82} \right). \quad (62)$$

Example 15. Reconsider Examples 4 and 5, but now with $S = 3$ sectors having front-to-back ratio $Q = 20$ dB. Shown in Fig. 9 are (62), the numerical mapping of $C(\rho)$ onto (59) for SISO and MIMO, and the simulated C_{exact} .

For any setting for which $C(\rho_S)$ is available, we can also compute the spatially averaged ergodic spectral efficiency as

$$\bar{C} = \int_0^{\frac{Q}{S-1}} C(\theta) dF_{\rho_S}(\theta). \quad (63)$$

Example 16. Let $\eta = 3.8$, $S = 3$ and $Q = 20$ dB. For SISO, $\bar{C} = 1.53$ b/s/Hz per sector, which adds up to 4.59 b/s/Hz per BS. For $S = 1$, in contrast, a read-out of Fig. 5 gives $\bar{C} = 1.84$ b/s/Hz per BS. With the sector nonideality accounted for, the overall spectral efficiency of a SISO network gets multiplied by 2.5 when cells are split in three sectors.

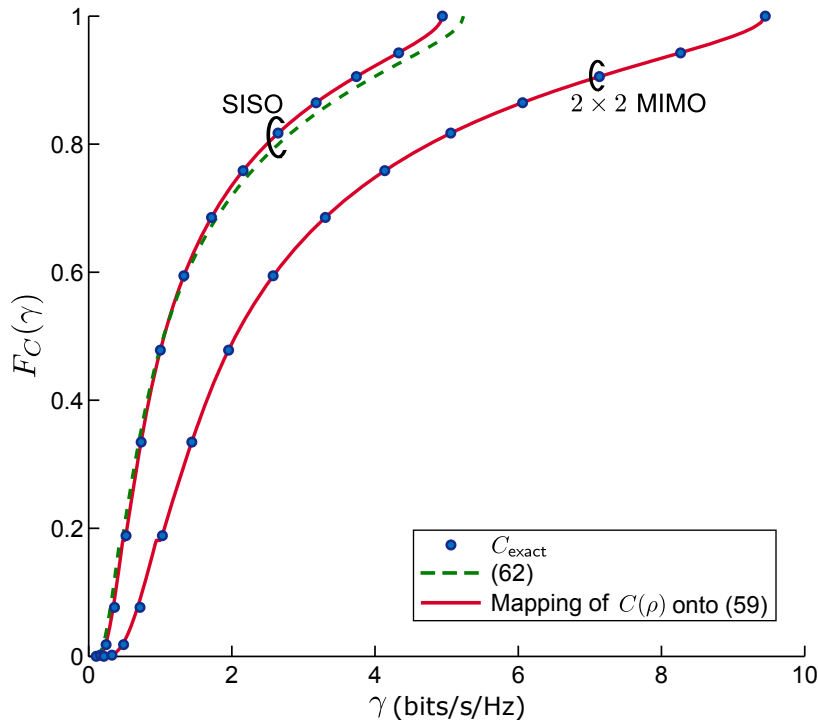


Fig. 9: CDF of ergodic spectral efficiency for $\eta = 3.8$, $S = 3$ and $Q = 20$ dB.

For 2×2 MIMO, in turn, $\bar{C} = 2.95$ b/s/Hz per sector adding up to 8.85 b/s/Hz per BS. The sectorization multiplier is 2.49, almost unchanged from its SISO value.

IX. APPLICATION TO LATTICE NETWORKS

Before wrapping up, we close the loop and verify the initial premise whereby a PPP model was invoked for the BS locations, confirming that such model is representative because of shadowing. To that end, we compare our PPP-based analytical results with Monte-Carlo simulations for settings at the extreme end of the point process spectrum, namely regular lattices.

Example 17. Shown in Fig. 10 is $F_C(\cdot)$ as given in (27) for SISO, in comparison with the results for a lattice of 977 hexagonal cells with $\eta = 4$ and various values of σ_{dB} . The convergence is conspicuous and, most importantly, the agreement is excellent for typical outdoor values of σ_{dB} , in the range of 10–12 dB.

Example 18. The comparison of Fig. 10 is repeated, for $S = 3$ sectors and $Q = 20$ dB, in Fig. 11, with similar observations in terms of the convergence.

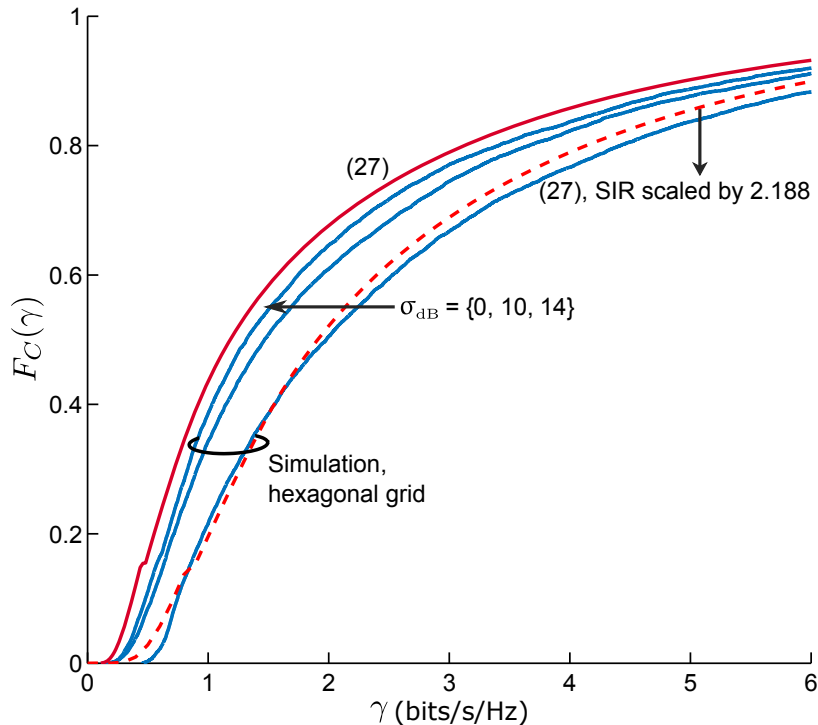


Fig. 10: CDF of SISO ergodic spectral efficiency with no sectorization ($S = 1$): PPP-based analytical result vs Monte-Carlo over a lattice network of hexagonal cells with $\sigma_{\text{dB}} = 0$ dB, 10 dB and 14 dB. The dashed curve corresponds to using $F_\rho(\theta/2.188)$ in lieu of $F_\rho(\theta)$ and proceeding as if the network conformed to a PPP. In all cases, $\eta = 4$.

Example 19. Shown in Fig. 12 is \bar{C} as given in (44), for SISO, in comparison with the results for a lattice of 977 hexagonal cells with various values of σ_{dB} and η .

Further reinforcing the relevance of PPP-based results to lattice networks, it has been argued in [60]–[62] that the SINR distribution of a shadowless lattice network is essentially a shifted version of its PPP counterpart, i.e., a shifted version of the SINR distribution for asymptotically strong shadowing. Moreover, this shift does not depend on the path loss exponent, but only on the type of lattice.

Example 20. For a triangular lattice (hexagonal cells), the shift to apply is $10 \log_{10} 2.188 = 3.4$ dB [60]–[62]. Shown in Fig. 10 is $F_C(\cdot)$ recomputed with $F_\rho(\theta/2.188)$ in lieu of $F_\rho(\theta)$, and the agreement with $F_C(\cdot)$ for a network of hexagonal cells and no shadowing is highly satisfactory.

Altogether then, PPP results enable characterizing the distributions of SINR and spectral efficiency both with (asymptotically strong) and without shadowing, bracketing the range of

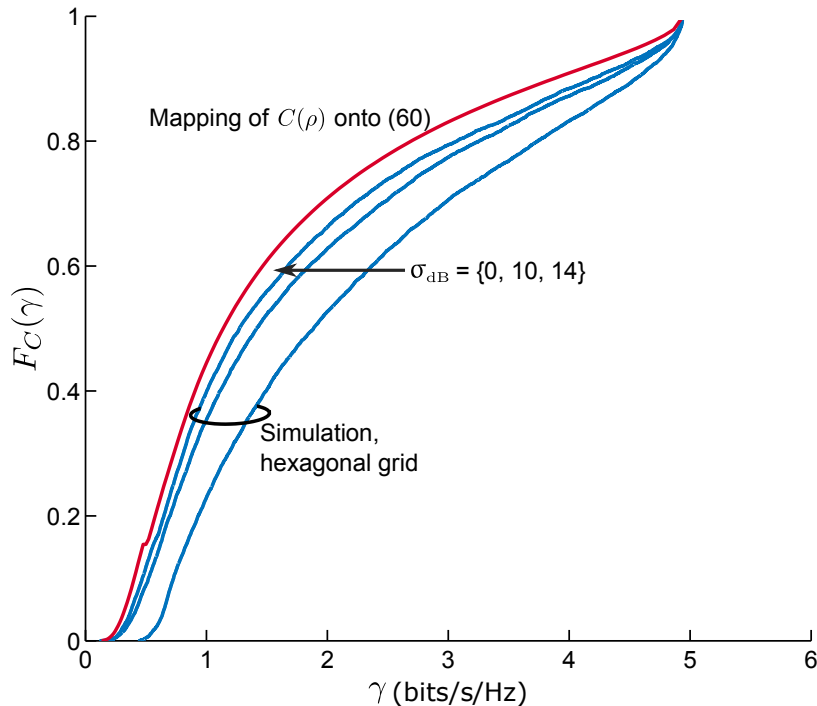


Fig. 11: CDF of SISO ergodic spectral efficiency with $S = 3$ sectors and $Q = 20$ dB: PPP-based analytical result vs Monte-Carlo over a lattice network of hexagonal cells with $\sigma_{\text{dB}} = 0$ dB, 10 dB and 14 dB. In all cases, $\eta = 4$.

values that a given network can exhibit over all possible shadowing strengths.

X. SUMMARY

By decoupling small- and large-scale channel features and abstracting the former via local ergodicity, the stochastic geometry analysis of wireless networks can focus crisply on the large-scale properties. Jointly with a Gaussian model for the aggregate interference that recognizes that the fading of each term therein is unknown, this enables circumventing analytical roadblocks and deriving expressions that are more open to generalization, readily accommodating aspects such as MIMO or sectorization. The obtained spectral efficiencies lower-bound the exact values with a degree of accuracy that justifies writing $C \lesssim C_{\text{exact}}$.

Thanks to the PPP-likeness brought about by shadowing, the obtained expressions apply to any stationary and ergodic network model exhibiting reasonable shadowing strengths. Furthermore, with a proper shift, these expressions apply to shadowless networks, which are relevant insofar as they can model planned deployments where the BS locations do depend on the radio propagation. Thus, PPP analysis can serve to bracket the entire performance range in a given environment.

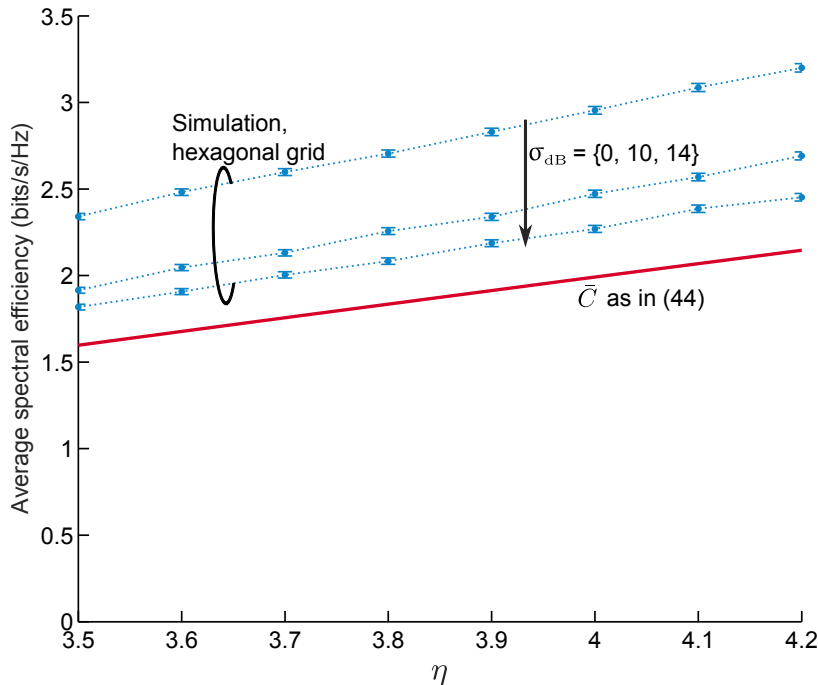


Fig. 12: Spatially averaged SISO ergodic spectral efficiency as function of η with no sectorization ($S = 1$): PPP-based analytical result vs Monte-Carlo over a lattice network of hexagonal cells with $\sigma_{\text{dB}} = 0$ dB, 10 dB and 14 dB. The error bars around the simulation results indicate the 99% confidence interval.

The approach propounded in this paper is extensible to settings where noise is nonnegligible, and the accuracy of the results could then only improve even further since our interference model is an exact match for Gaussian noise devoid of fading.

Besides the addition of noise, numerous other extensions are invited, for instance multiuser MIMO or BS cooperation [63]. When dealing with MIMO, care must be exercised whenever $N_r > N_t$ and, especially, whenever $N_r \gg N_t$; then, if the fading of dominant interferer(s) can be tracked, spatial color can be exploited [64], [65]. This can be accounted for by circumscribing our unfaded interference model to the rest of the interference, separately incorporating the terms that correspond to interferers whose fading is known.

ACKNOWLEDGMENT

Motivating discussions with Prof. Jeffrey G. Andrews are gratefully acknowledged. The efficient editorial handling by Dr. Bruno Clerckx and the excellent feedback provided by the reviewers are also gratefully acknowledged.

APPENDIX A
COMPUTATION OF C_{exact}

For given $\{r_k\}_{k \in \mathbb{N}_0}$ and H_0 , the exact mutual information under the non-Gaussian z in (2) is

$$I\left(s_0; \sqrt{P r_0^{-\eta}} H_0 s_0 + z\right) = \mathfrak{h}\left(\sqrt{P r_0^{-\eta}} H_0 s_0 + z\right) - \mathfrak{h}\left(\sqrt{P r_0^{-\eta}} H_0 s_0 + z \mid s_0\right) \quad (64)$$

$$= \mathfrak{h}\left(\sqrt{P r_0^{-\eta}} H_0 s_0 + z\right) - \mathfrak{h}(z) \quad (65)$$

where we have introduced the differential entropy $\mathfrak{h}(x) = -\mathbb{E}[\log f_{\mathbf{x}'}(\mathbf{x}')] with $\mathbf{x}' = [\Re(x) \Im(x)]^T$. The expectations are evaluated via Monte-Carlo over the random variables $\{s_k\}_{k \in \mathbb{N}_0}$ and $\{H_k\}_{k \in \mathbb{N}}$, and averaged over multiple realizations of H_0 to obtain C_{exact} in (6). The large-scale distribution of C_{exact} , and its average \bar{C}_{exact} , are obtained via multiple realizations of $\{r_k\}_{k \in \mathbb{N}_0}$.$

With MIMO, the foregoing computation involves channel matrices and signal vectors, with the differential entropy of a vector $\mathbf{x} \in \mathbb{C}^n$ being $\mathfrak{h}(\mathbf{x}) = -\mathbb{E}[\log f_{\mathbf{x}''}(\mathbf{x}'')] with $\mathbf{x}'' = [\Re(\mathbf{x}^T) \Im(\mathbf{x}^T)]^T$.$

APPENDIX B
DERIVATION OF (28)

With SINR given by (3),

$$\mathbb{E}[\log_2(1 + \text{SINR}|\{r_k\}_{k=0}^\infty)] = \int_0^\infty \mathbb{P}[\log_2(1 + \text{SINR}|\{r_k\}_{k=0}^\infty) > y] dy \quad (66)$$

$$= \int_0^\infty \frac{\log_2 e}{1+x} F_{\text{SINR}|\{r_k\}}^c(x) dx \quad (67)$$

where (67) follows from the variable change $y = \log_2(1+x)$ and the CCDF $F_{\text{SINR}|\{r_k\}}^c(\cdot)$ can be computed as

$$F_{\text{SINR}|\{r_k\}}^c(x) = \mathbb{P}\left[\frac{P r_0^{-\eta} |H_0|^2}{P \sum_{k=1}^\infty r_k^{-\eta} |H_k|^2 + N_0} > x \mid \{r_k\}_{k=0}^\infty\right] \quad (68)$$

$$= \mathbb{E}\left[e^{-x r_0^\eta (\sum_{k=1}^\infty r_k^{-\eta} |H_k|^2 + N_0/P)} \mid \{r_k\}_{k=0}^\infty\right] \quad (69)$$

$$= e^{-x r_0^\eta N_0/P} \mathbb{E}\left[\prod_{k=1}^\infty e^{-x r_0^\eta r_k^{-\eta} |H_k|^2} \mid \{r_k\}_{k=0}^\infty\right] \quad (70)$$

$$= e^{-x r_0^\eta N_0/P} \prod_{k=1}^\infty \frac{1}{1+x(r_0/r_k)^\eta} \quad (71)$$

where (69) follows from the exponential distribution of $|H_0|^2$ and the expectation is over $\{H_k\}_{k=1}^\infty$. In turn, (71) follows from the fact that $\{H_k\}_{k=1}^\infty$ are IID.

APPENDIX C

DERIVATIONS OF (44), (49) AND (51)

Plugging the PDF obtained by differentiating (23) into (43),

$$\bar{C} \approx \int_0^{\frac{s^*}{\log(1-\text{sinc } \delta)}} C(\theta) \frac{-e^{s^*/\theta} s^*}{\theta^2} d\theta + \int_1^\infty C(\theta) \frac{\delta \text{sinc } \delta}{\theta^{\delta+1}} d\theta. \quad (72)$$

From $C(\cdot)$ as given in (15) and (30), the above integrals yield (44) and (49), respectively. These integrations are facilitated by invoking $E_1(x) = -E_i(-x)$, where $E_i(x) = \int_{-x}^\infty \frac{-e^{-t}}{t} dt$, in conjunction with the identities given in [66] with appropriate variable changes.

Similarly, from $C(\cdot)$ as given in (50), integration by parts in (72) using the identities [67, 2.325.6], [67, 2.325.7], [67, 2.728.1] and [67, 3.194.2] with appropriate variable changes gives the expression claimed in (51).

REFERENCES

- [1] J. G. Andrews, F. Baccelli, and R. K. Ganti, "A tractable approach to coverage and rate in cellular networks," *IEEE Trans. Commun.*, vol. 59, no. 11, pp. 3122–3134, Nov. 2011.
- [2] B. Błaszczyszyn, M. K. Karray, and H. P. Keeler, "Wireless networks appear Poissonian due to strong shadowing," *IEEE Trans. Wireless Commun.*, vol. 14, no. 8, pp. 4379–4390, Aug. 2015.
- [3] H. P. Keeler, N. Ross, and A. Xia, "When do wireless network signals appear Poisson?" 2014. [Online]. Available: <http://arxiv.org/abs/1411.3757>
- [4] J. G. Andrews, S. Buzzi, W. Choi, S. Hanly, A. Lozano, A. C. K. Soong, and J. C. Zhang, "What will 5G be?" *IEEE J. Select. Areas Commun.*, vol. 32, no. 6, pp. 1065–1082, Jul. 2014.
- [5] F. Boccardi, R. W. Heath Jr., A. Lozano, T. Marzetta, and P. Popovski, "Five disruptive technology directions for 5G," *IEEE Commun. Mag.*, vol. 52, no. 2, pp. 74–80, Feb. 2014.
- [6] M. Haenggi, J. G. Andrews, F. Baccelli, O. Dousse, and M. Franceschetti, "Stochastic geometry and random graphs for the analysis and design of wireless networks," *IEEE J. Select. Areas Commun.*, vol. 27, no. 7, pp. 1029–1046, May 2009.
- [7] P. C. Pinto and M. Z. Win, "Communication in a Poisson field of interferers—part I: Interference distribution and error probability," *IEEE Trans. Wireless Commun.*, vol. 9, no. 7, pp. 2176–2186, Jul. 2010.
- [8] —, "Communication in a Poisson field of interferers—part II: Channel capacity and interference spectrum," *IEEE Trans. Wireless Commun.*, vol. 9, no. 7, pp. 2187–2195, Jul. 2010.
- [9] M. Haenggi, *Stochastic Geometry for Wireless Networks*. Cambridge, UK: Cambridge University Press, 2012.
- [10] N. Deng, W. Zhou, and M. Haenggi, "The Ginibre point process as a model for wireless networks with repulsion," *IEEE Trans. Wireless Commun.*, vol. 14, no. 1, pp. 107–121, Jan. 2015.
- [11] J. S. Gomez, A. Vasseur, A. Vergne, P. Martins, L. Decreusefond, and W. Chen, "A case study on regularity in cellular network deployment," *IEEE Wireless Commun. Lett.*, vol. 4, pp. 421–424, Aug. 2015.
- [12] A. Guo and M. Haenggi, "Joint spatial and propagation models for cellular networks," in *Proc. IEEE Global Telecommun. Conf.*, Dec. 2015, pp. 1–6.

- [13] J. G. Andrews, R. K. Ganti, M. Haenggi, N. Jindal, and S. Weber, "A primer on spatial modeling and analysis in wireless networks," *IEEE Commun. Mag.*, vol. 48, pp. 156–163, Nov. 2010.
- [14] H. S. Dhillon, R. K. Ganti, F. Baccelli, and J. G. Andrews, "Modeling and analysis of K -tier downlink heterogeneous cellular networks," *IEEE J. Select. Areas Commun.*, vol. 30, no. 3, pp. 550–560, Apr. 2012.
- [15] S. Mukherjee, "Distribution of downlink SINR in heterogeneous cellular networks," *IEEE J. Select. Areas Commun.*, vol. 30, no. 3, pp. 575–585, Apr. 2012.
- [16] S. Singh, H. S. Dhillon, and J. G. Andrews, "Offloading in heterogeneous networks: Modeling, analysis, and design insights," *IEEE Trans. Wireless Commun.*, vol. 12, no. 5, pp. 2484–2497, May 2013.
- [17] H. ElSawy, E. Hossain, and M. Haenggi, "Stochastic geometry for modeling, analysis, and design of multi-tier and cognitive cellular wireless networks: A survey," *IEEE Commun. Surveys Tuts.*, vol. 15, no. 3, pp. 996–1019, Third Quarter 2013.
- [18] C. H. Lee and M. Haenggi, "Interference and outage in Poisson cognitive networks," *IEEE Trans. Wireless Commun.*, vol. 11, no. 4, pp. 1392–1401, Apr. 2012.
- [19] B. Błaszczyszyn and M. K. Karray, "Spatial distribution of the SINR in Poisson cellular networks with sector antennas," *IEEE Trans. Wireless Commun.*, vol. 15, pp. 581–593, Jan. 2016.
- [20] A. Guo and M. Haenggi, "Asymptotic deployment gain: A simple approach to characterize the SINR distribution in general cellular networks," *IEEE Trans. Commun.*, vol. 63, pp. 962–976, Mar. 2015.
- [21] M. D. Renzo and P. Guan, "Stochastic geometry modeling and system-level analysis of uplink heterogeneous cellular networks with multi-antenna base stations," *IEEE Trans. Commun.*, vol. 64, pp. 2453–2476, Jun. 2016.
- [22] M. D. Renzo and W. Lu, "Stochastic geometry modeling and performance evaluation of MIMO cellular networks using the equivalent-in-distribution (EiD)-based approach," *IEEE Trans. Commun.*, vol. 63, pp. 977–996, Mar. 2015.
- [23] H. S. Dhillon, M. Kountouris, and J. G. Andrews, "Downlink MIMO HetNets: Modeling, ordering results and performance analysis," *IEEE Trans. Wireless Commun.*, vol. 12, pp. 5208–5222, Oct. 2013.
- [24] L. H. Afify, H. ElSawy, T. Y. Al-Naffouri, and M.-S. Alouini, "Unified stochastic geometry model for MIMO cellular networks with retransmissions," *IEEE Trans. Commun.*, 2016, to be published. [Online]. Available: <http://ieeexplore.ieee.org/stamp/stamp.jsp?arnumber=7588201>
- [25] C. Li, J. Zhang, J. G. Andrews, and K. B. Letaief, "Success probability and area spectral efficiency in multiuser MIMO HetNets," *IEEE Trans. Commun.*, vol. 64, no. 4, pp. 1544–1556, Apr. 2016.
- [26] R. Tanbourgi, H. S. Dhillon, and F. K. Jondral, "Analysis of joint transmit–receive diversity in downlink MIMO heterogeneous cellular networks," *IEEE Trans. Wireless Commun.*, vol. 14, no. 12, pp. 6695–6709, Dec. 2015.
- [27] R. Tanbourgi, S. Singh, J. G. Andrews, and F. K. Jondral, "A tractable model for noncoherent joint-transmission base station cooperation," *IEEE Trans. Wireless Commun.*, vol. 13, no. 9, pp. 4959–4973, Sep. 2014.
- [28] A. Lozano and N. Jindal, "Transmit diversity vs. spatial multiplexing in modern MIMO systems," *IEEE Trans. Wireless Commun.*, vol. 9, no. 1, pp. 186–197, Jan. 2010.
- [29] —, "Are yesterday's information-theoretic fading models and performance metrics adequate for the analysis of today's wireless systems?" *IEEE Commun. Mag.*, vol. 50, no. 11, pp. 210–217, Nov. 2012.
- [30] W. C. Jakes, *Microwave mobile communications*. Wiley-IEEE Press, 1994.
- [31] N. Ross and D. Schuhmacher, "Wireless network signals with moderately correlated shadowing still appear Poisson," 2016, arXiv:1606.05825 [cs.NI].
- [32] M. Haenggi, "A geometric interpretation of fading in wireless networks: Theory and applications," *IEEE Trans. Inform. Theory*, vol. 54, pp. 5500–5510, Dec. 2008.

- [33] P. Madhusudhanan, J. G. Restrepo, Y. E. Liu, and T. X. Brown, "Carrier to interference ratio analysis for the shotgun cellular system," in *Proc. IEEE Global Telecommun. Conf.*, Nov. 2009, pp. 1–6.
- [34] B. Błaszczyszyn, M. K. Karray, and F.-X. Klepper, "Impact of the geometry, path-loss exponent and random shadowing on the mean interference factor in wireless cellular networks," in *Proc. IFIP Wireless and Mobile Networking Conference (WMNC)*, Budapest, Hungary, Oct. 2010, pp. 1–6.
- [35] X. Zhang and M. Haenggi, "A stochastic geometry analysis of inter-cell interference coordination and intra-cell diversity," *IEEE Trans. Wireless Commun.*, vol. 13, pp. 6655–6669, Dec. 2014.
- [36] A. Guo and M. Haenggi, "Spatial stochastic models and metrics for the structure of base stations in cellular networks," *IEEE Trans. Wireless Commun.*, vol. 12, pp. 5800–5812, Nov. 2013.
- [37] N. Deng, W. Zhou, and M. Haenggi, "Heterogeneous cellular network models with dependence," *IEEE J. Select. Areas Commun.*, vol. 33, no. 10, pp. 2167–2181, Oct. 2015.
- [38] M. Afshang and H. S. Dhillon, "Spatial modeling of device-to-device networks: Poisson cluster process meets Poisson hole process," in *Proc. Annual Asilomar Conf. Signals, Syst., Comp.*, Pacific Grove, CA, Nov. 2015, pp. 317–321.
- [39] C. Saha, M. Afshang, and H. S. Dhillon, "Enriched K-tier HetNet model to enable the analysis of user-centric small cell deployments," 2016. [Online]. Available: <http://arxiv.org/abs/1606.06223>
- [40] A. Lapidoto and S. Shamai, "Fading channels: how perfect need "perfect side information" be?" *IEEE Trans. on Inform. Theory*, vol. 48, no. 5, pp. 1118–1134, 2002.
- [41] A. Giorgetti and M. Chiani, "Influence of fading on the Gaussian approximation for BPSK and QPSK with asynchronous cochannel interference," *IEEE Trans. on Wireless Communications*, vol. 4, pp. 384–389, Mar. 2005.
- [42] S. Ak, H. Inaltekin, and H. V. Poor, "Gaussian approximation for the downlink interference in heterogeneous cellular networks," 2016. [Online]. Available: <http://arxiv.org/abs/1601.06023>
- [43] R. K. Mungara, D. Morales-Jiménez, and A. Lozano, "System-level performance of interference alignment," *IEEE Trans. Wireless Commun.*, vol. 14, no. 2, pp. 1060–1070, Feb. 2015.
- [44] G. George, R. K. Mungara, and A. Lozano, "An analytical framework for device-to-device communication in cellular networks," *IEEE Trans. Wireless Commun.*, vol. 14, no. 11, pp. 6297–6310, Nov. 2015.
- [45] S. N. Diggavi and T. M. Cover, "The worst additive noise under a covariance constraint," *IEEE Trans. on Inform. Theory*, vol. 47, no. 7, pp. 3072–3081, 2001.
- [46] H. Shin and J. H. Lee, "Capacity of multiple-antenna fading channels: spatial fading correlation, double scattering, and keyhole," *IEEE Trans. Inform. Theory*, vol. 49, no. 10, pp. 2636–2647, Oct. 2003.
- [47] M. Haenggi, "On distances in uniformly random networks," *IEEE Trans. Inform. Theory*, vol. 51, pp. 3584–3586, Oct. 2005.
- [48] M. Zorzi, "On the analytical computation of the interference statistics with applications to the performance evaluation of mobile radio systems," *IEEE Trans. Commun.*, vol. 45, no. 1, pp. 103–109, Jan. 1997.
- [49] R. Nasri and A. Jaziri, "Analytical tractability of hexagonal network model with random user location," *IEEE Trans. Wireless Commun.*, vol. 15, no. 5, pp. 3768–3780, May 2016.
- [50] B. Błaszczyszyn, M. K. Karray, and H. P. Keeler, "Using Poisson processes to model lattice cellular networks," in *Proc. IEEE INFOCOM*, Apr. 2013, pp. 773–781.
- [51] S. Mukherjee, "Downlink SINR distribution in a heterogeneous cellular wireless network with max-SINR connectivity," in *Proc. Annual Allerton Conf. Commun., Cont., Computing*, Sep. 2011, pp. 1649–1656.

- [52] B. Błaszczyszyn and H. P. Keeler, "Studying the SINR process of the typical user in Poisson networks using its factorial moment measures," *IEEE Trans. Inform. Theory*, vol. 61, no. 12, pp. 6774–6794, Dec 2015.
- [53] P. Madhusudhanan, J. G. Restrepo, Y. Liu, T. X. Brown, and K. R. Baker, "Downlink performance analysis for a generalized shotgun cellular system," *IEEE Trans. Wireless Commun.*, vol. 13, no. 12, pp. 6684–6696, Dec. 2014.
- [54] R. K. Ganti and M. Haenggi, "SIR asymptotics in Poisson cellular networks without fading and with partial fading," in *Proc. IEEE Int. Conf. Commun.*, May 2016.
- [55] S. Catreux, P. F. Driessen, and L. J. Greenstein, "Data throughputs using multiple-input multiple-output (MIMO) techniques in a noise-limited cellular environment," *IEEE Trans. Wireless Commun.*, vol. 1, no. 2, pp. 226–235, Apr. 2002.
- [56] A. K. Gupta, H. S. Dhillon, S. Vishwanath, and J. G. Andrews, "Downlink multi-antenna heterogeneous cellular network with load balancing," *IEEE Trans. Commun.*, vol. 62, pp. 4052–4067, Nov. 2014.
- [57] H. ElSawy, A. Sultan-Salem, M.-S. Alouini, and M. Z. Win, "Modeling and analysis of cellular networks using stochastic geometry: A tutorial," 2016. [Online]. Available: <http://arxiv.org/abs/1604.03689/>
- [58] A. Lozano, A. M. Tulino, and S. Verdú, "Multiple-antenna capacity in the low-power regime," *IEEE Trans. on Information Theory*, vol. 49, no. 10, pp. 2527–2544, 2003.
- [59] W. Koepf, "Hypergeometric summation: An algorithmic approach to summation and special function identities," *American Mathematical Society, Providence, RI*, 1998.
- [60] A. Guo and M. Haenggi, "Asymptotic deployment gain: A simple approach to characterize the SINR distribution in general cellular networks," *IEEE Trans. Commun.*, vol. 63, no. 3, pp. 962–976, Mar. 2015.
- [61] M. Haenggi, "The mean interference-to-signal ratio and its key role in cellular and amorphous networks," *IEEE Wireless Commun. Lett.*, vol. 3, no. 6, pp. 597–600, Dec. 2014.
- [62] R. K. Ganti and M. Haenggi, "Asymptotics and approximation of the SIR distribution in general cellular networks," *IEEE Trans. Wireless Commun.*, vol. 15, no. 3, pp. 2130–2143, Mar. 2016.
- [63] A. Lozano, R. W. Heath Jr., and J. G. Andrews, "Fundamental limits of cooperation," *IEEE Trans. Inform. Theory*, vol. 59, pp. 5213–5226, Sept. 2013.
- [64] A. Lozano and A. M. Tulino, "Capacity of multiple-transmit multiple-receive antenna architectures," *IEEE Trans. Inform. Theory*, vol. 48, pp. 3117–3128, Dec. 2002.
- [65] J. Lee, N. Lee, and F. Baccelli, "Scaling laws for ergodic spectral efficiency in mimo poisson networks," 2016, arXiv:1608.06065 [cs.IT], Aug.
- [66] "The Wolfram functions website," Wolfram Res., Champaign, IL, USA, 2001. [Online]. Available: <http://functions.wolfram.com/GammaBetaErf/ExpIntegralEi/21/01/02/02/01/ShowAll.html>
- [67] I. S. Gradshteyn and I. M. Ryzhik, *Table of Integrals, Series, and Products*. Academic Press, San Diego, 7th Ed., 2007.